Noninternalizing Monoclonal Antibodies Are Suitable Candidates for ^{125}I Radioimmunotherapy of Small-Volume Peritoneal Carcinomatosis

Lore Santoro[1–4], Samir Boutaleb[1–4], Véronique Garambois[1–4], Caroline Bascoul-Mollevi[4], Vincent Boudousq[1–5], Pierre-Olivier Kotzki[1–5], Monique Pèlegrin[1–4], Isabelle Navarro-Teulon[1–4], André Pèlegrin[1–4], and Jean-Pierre Pouget[1–4,6]

[1]Institut de Recherche en Cancérologie de Montpellier, Montpellier, France; [2]INSERM, U896, Montpellier, France; [3]Université Montpellier 1, Montpellier, France; [4]CRLC Val d'Aurelle-Paul Lamarque, Montpellier, France; [5]Service de Médecine Nucléaire, CHU de Nîmes, Nîmes, France; and [6]Direction de la Radioprotection de l'Homme, Institut de Radioprotection et de Sûreté Nucléaire, Fontenay-aux-Roses, France

We have previously shown that, in vitro, monoclonal antibodies (mAbs) labeled with the Auger electron emitter ^{125}I are more cytotoxic if they remain at the cell surface and do not internalize in the cytoplasm. Here, we assessed the in vivo biologic efficiency of internalizing and noninternalizing ^{125}I-labeled mAbs for the treatment of small solid tumors. **Methods:** Swiss nude mice bearing intraperitoneal tumor cell xenografts were injected with 37 MBq (370 MBq/mg) of internalizing (anti-*HER1*) ^{125}I-m225 or noninternalizing (anti-CEA) ^{125}I-35A7 mAbs at days 4 and 7 after tumor cell grafting. Nonspecific toxicity was assessed using the irrelevant ^{125}I-PX mAb, and untreated controls were injected with NaCl. Tumor growth was followed by bioluminescence imaging. Mice were sacrificed when the bioluminescence signal reached 4.5×10^7 photons/s. Biodistribution analysis was performed to determine the activity contained in healthy organs and tumor nodules, and total cumulative decays were calculated. These values were used to calculate the irradiation dose by the MIRD formalism. **Results:** Median survival (MS) was 19 d in the NaCl-treated group. Similar values were obtained in mice treated with unlabeled PX (MS, 24 d) and 35A7 (MS, 24 d) or with ^{125}I-PX mAbs (MS, 17 d). Conversely, mice treated with unlabeled or labeled internalizing m225 mAb (MS, 76 and 77 d, respectively) and mice injected with ^{125}I-35A7 mAb (MS, 59 d) showed a significant increase in survival. Irradiation doses were comparable in all healthy organs, independently from the mAb used, whereas in tumors the irradiation dose was 7.4-fold higher with ^{125}I-labeled noninternalizing than with internalizing mAbs. This discrepancy might be due to iodotyrosine moiety release occurring during the catabolism of internalizing mAbs associated with high turnover rate. **Conclusion:** This study indicates that ^{125}I-labeled noninternalizing mAbs could be suitable for radioimmunotherapy of small solid tumors and that the use of internalizing mAbs should not be considered as a requirement for the success of treatments with ^{125}I Auger electrons.

Received Jun. 5, 2009; revision accepted Sep. 2, 2009.
For correspondence or reprints contact: Jean-Pierre Pouget, Institut de Recherche en Cancérologie de Montpellier, CRLC Val d'Aurelle, 34298 Montpellier Cedex 5, France.
E-mail: jean-pierre.pouget@valdorel.fnclcc.fr

Key Words: radioimmunotherapy; Auger electrons; solid tumors
J Nucl Med 2009; 50:2033–2041
DOI: 10.2967/jnumed.109.066993

The development of clinically effective radiolabeled monoclonal antibodies (mAbs) has been limited to the treatment of lymphomas. Indeed, only ibritumomab tiuxetan (Zevalin; Biogen IDEC Pharmaceuticals Corporation) and tositumomab (Bexxar; Corixa and GlaxoSmithKline Corporations), 2 anti-CD20 mAbs conjugated to ^{90}Y and ^{131}I, respectively, have been approved by the Food and Drug Administration for the therapy of lymphomas (*1*). Conversely, the few candidates for the therapy of solid tumors that have progressed to phase III clinical trials have not given clear-cut results (*2–4*).

This lack of progression to phase III trials can be explained by inhomogeneous targeting related to poor vascularization and high interstitial pressure due to insufficient lymphatic drainage (*5–9*). Uptake of radioactivity in solid tumors is generally between 0.001% and 0.01% of the injected dose per gram of tumor and is inversely proportional to the size of the tumor. In addition, solid tumors show low sensitivity to radiation. Therefore, myelotoxicity is usually attained before the dose required for tumor eradication is reached inside the cancer mass. Consequently, it is now admitted that, in the case of solid tumors, radioimmunotherapy should be considered only for the treatment of small tumors (*10,11*), microscopic residual disease, or metastasis (*12*).

The other issue concerns the choice of emitter used to label the mAbs. The 2 strong-energy β-emitters (i.e., ^{90}Y and ^{131}I) produce electrons having ranges between 2 and 10 mm, respectively. The long range of energetic β-particle of ^{90}Y

and γ-rays associated with ^{131}I are responsible for nonspecific irradiation that may cause undesirable effects such as myelosuppression. However, in mice, several studies showed that ^{131}I-mAbs could efficiently treat micrometastases (<1 mm) but not tumors of 2–3 mm (*13,14*). Other emitters, such as high-linear-energy-transfer (LET) particles, may be more attractive candidates for the therapy of solid tumors. They include α- and Auger electron–emitting radionuclides. α-Emitters, which are suitable for radioimmunotherapy, include mostly ^{212}Bi or ^{225}Ac/^{213}Bi and ^{211}At. α-Particles have a short path length (<100 μm) that minimizes damage to normal tissues. They also possess a high LET, with an energy deposit of about 100 keV/μm, compared with 0.2 keV/μm for the β-emitters (*15*). However, the use of α-particles in radioimmunotherapy requires the development of cost-effective radionuclide production and protein-labeling chemistry. Another drawback of α-emitters is the production of radioactive daughter isotopes that can hardly be withheld in a chelator and tend to escape from targeted cells and accumulate in bone (*16*).

By contrast, Auger electron emitters are available for clinical use. Although the energy of an Auger electron ranges from a few electron volts to about 20–25 keV, those with high-LET characteristics (i.e., between 4 and 26 keV/μm) (*17*) have an energy comprising between a few 10s of electron volts and 1 keV, and their path length in biologic tissues ranges from about 2 to 500 nm. Therefore, in this work we used the term *low-energy Auger electrons* to indicate this category of Auger electrons with high-LET features. Several studies underscored the advantages of such emitters in comparison to conventional ^{131}I and ^{90}Y in radioimmunotherapy of solid tumors because of their much less toxic side effects (*18–21*). However, because of their short path length, their final localization within the cell has to be considered. Many studies using ^{125}I-iododeoxyuridine highlighted the requirement for the emitter to be located within the DNA molecule to observe a cellular toxicity similar to that of α-particles (*22*). However, in radioimmunotherapy, the final localization of radiolabeled mAbs is either the cytoplasm or the cell surface, depending on whether internalizing or noninternalizing mAbs are used. We previously showed that, in vitro, noninternalizing ^{125}I-mAbs were more harmful than internalizing ones. Although the strongest toxicity of ^{125}I is observed when the isotope is incorporated within the DNA molecule (*17,23,24*), these results suggest that the cell membrane also is a sensitive target (*25*). Here, we investigated the efficacy of noninternalizing and internalizing ^{125}I-mAbs in the treatment of mice with tumor cell xenografts. For this purpose, nude mice bearing intraperitoneal A-431–derived tumors were injected twice with 37 MBq of internalizing or noninternalizing ^{125}I-mAbs. Tumor growth was followed by bioluminescence imaging, and the endpoint was a bioluminescence signal of 4.5×10^7 photons/s. Our results demonstrate that ^{125}I-mAbs are an efficient tool for the treatment of small solid tumors and that the use of internalizing ^{125}I-mAb is not a prerequisite for radioimmunotherapy.

MATERIALS AND METHODS

Cell Line and mAbs

The vulvar squamous carcinoma cell line A-431 expressing the epidermal growth factor receptor (EGFR or *HER1*) was transfected with vectors encoding for the carcinoembryonic antigen (CEA) gene as described by Pelegrin et al. (*26*) and for luciferase as described by Pillon et al. (*27*). Cells were grown as described by Pouget et al. (*25*), and medium was supplemented with 1% geneticin.

The mouse hybridoma cell line producing the m225 mAb, which binds to EGFR, was obtained from the American Type Culture Collection. The noninternalizing murine IgG1k 35A7 mAb, specific for the CEA Gold 2 epitope (*28*), was used to target CEA in transfected A-431 cells. The irrelevant PX antibody was used for control experiments. PX is an IgG1 mAb that has been purified from the mouse myeloma MOPC 21 (*29*). The m225, 35A7, and PX mAbs were obtained from mouse hybridoma ascites fluids by ammonium sulfate precipitation followed by ion exchange chromatography on DE52 cellulose (Whatman).

Radiolabeling for Therapy and Biodistribution Analysis

^{125}I and ^{131}I were from PerkinElmer, and mAbs were radiolabeled as described by Pouget et al. (*25*). Specific activity was generally around 370 MBq/mg. For radioimmunotherapy, 2 injections of 37 MBq (equivalent to 100 μg of mAb) were used. For biodistribution experiments, a solution containing 185 kBq of ^{125}I-mAbs together with 320 kBq of ^{131}I-mAbs was completed with unlabeled mAbs to a final amount of 100 μg of mAbs.

Immunoreactivity of ^{125}I-mAbs against CEA or EGFR was assessed in vitro by direct binding assays. The binding percentage was determined by measuring the antigen-bound radioactivity after 2 washes with phosphate-buffered saline and ranged from 70% to 90%.

Animals

Swiss nude mice (6- to 8-wk-old females) were obtained from Charles River and were acclimated for 1 wk before experimental use. They were housed at 22°C and 55% humidity with a light–dark cycle of 12 h. Food and water were available ad libitum. Body weight was determined weekly, and clinical examinations were performed throughout the study. Experiments were performed in compliance with the French guidelines for experimental animal studies (agreement B34-172-27).

Radioimmunotherapy Experiments and Tumor Imaging

For radioimmunotherapy experiments, Swiss nude mice were intraperitoneally grafted with 0.7×10^6 A-431 cells suspended in 0.3 mL of Dulbecco's modified Eagle's medium. Tumor growth was assessed by bioluminescence imaging 3 d after cell xenografting, and animals were segregated in homogeneous groups according to the type of treatment (i.e., NaCl, ^{125}I-m225, ^{125}I-35A7, and ^{125}I-PX or unlabeled m225, 35A7, and PX mAbs).

Then, 37 MBq of ^{125}I-mAbs (specific activity, 370 MBq/mg), NaCl, or unlabeled mAbs (100 μg) were intravenously injected at days 4 and 7 after the grafting. Tumor growth was followed weekly by bioluminescence imaging. Mice were sacrificed when the bioluminescence signal reached a value of 4.5×10^7 photons/s. In summary, 31 mice were included in the NaCl, 13 in the PX, 14

in the 35A7, 7 in the m225, 19 in the ^{125}I-PX, 12 in the ^{125}I-35A7, and 6 in the ^{125}I-m225 groups.

A third intravenous injection of ^{125}I-m225 or ^{125}I-35A7 mAbs was administered in 2 additional groups of mice ($n = 7$ for each ^{125}I-mAb) at day 10, and animals were followed until the bioluminescence signal reached a value of 4.5×10^7 photons/s or until death.

Bioluminescence Imaging

In vivo bioluminescence imaging was performed after intraperitoneal injection of luciferin (0.1 mg luciferin/g) and as described by Pillon et al. (*27*).

Biodistribution Experiments

On day 1, 48 Swiss nude mice were intraperitoneally grafted with 0.7×10^6 A-431 cells suspended in 0.3 mL of Dulbecco's modified Eagle's medium. Mice were then separated into 2 groups. Group 1 received a single intravenous injection of labeled mAbs at day 4, and group 2 received 2 intravenous injections (days 4 and 7). Injected solutions (250 μL) were made up of 100 μg of 35A7 or m225 mAbs containing 185 kBq of ^{125}I-mAb (specific activity, 370 MBq/mg) and 100 μg of irrelevant PX mAb containing 320 kBq of ^{131}I-PX (specific activity, 370 MBq/mg). Mice in group 1 were sacrificed at 1, 24, 48, 72, 96, and 168 h after the injection, and mice from group 2 were sacrificed at the same time points but after the second injection. At each time point, animals were anesthetized and images were acquired; then the mice were euthanized, bled, and dissected. Blood, tumor nodules, and organs were weighed, and the uptake of radioactivity (i.e., $UOR_{Biodistribution}$ [UOR_{Biodis}]) was measured with a γ-well counter. Dual-isotope counting, ^{125}I versus ^{131}I, was done. The percentage of injected activity per gram of tissue (%IA/g), corrected for the radioactive decay, was calculated. For time points later than 72 h (i.e., after the second injection), the injected activity of group 2 was defined as the sum of the residual radioactivity due to injection 1 and of the radioactivity due to injection 2. We assumed that the radioactivity detected in the different organs of mice from group 1 after this time point was not specifically bound to receptors any longer and could be mobilized again in the blood circulation. Four mice were used for each time point.

In addition, a control group of mice injected only with NaCl was sacrificed at the same time points as the animals used for the biodistribution analysis, to follow the natural growth of the tumors.

Tumor Weight Assessment

In radioimmunotherapy experiments, tumor size could not be directly measured because direct measurement required mouse sacrifice and also because of the high activities. Therefore, we used the intensity of the bioluminescence signal collected weekly after tumor grafting to determine tumor size. To do this, we used biodistribution data to calibrate the bioluminescence signal (photons/s) as a function of tumor size. The values of the bioluminescence signal of tumor nodules were collected at different time points during the biodistribution analysis and plotted versus their weight directly determined as follows. Initially, tumor nodules were weighed. However, these values appeared to be less accurate than estimation from size measurement because of blood or water content or contamination by other tissues. Therefore, their length, width, and depth were measured at each time point of the biodistribution study and used for volume determination. A density of 1.05 g/cm^3 was then used for calculating the weight of each nodule.

Uptake of Radioactivity Per Organ and Tumor

The uptake of radioactivity per tissue (expressed in becquerels) in radioimmunotherapy experiments ($UOR_{radioimmunotherapy}$ [UOR_{RIT}]) was extrapolated from the uptake per tissue (UOR_{Biodis}) measured during biodistribution experiments. Because activities used in radioimmunotherapy experiments were 200 times higher than those used in biodistribution analysis for the same amount of injected mAbs (100 μg), all the UOR_{Biodis} values were multiplied by 200 to mimic the therapeutic conditions. We considered that the weight of healthy tissues did not change all along the study period and did not differ between radioimmunotherapy and biodistribution experimental conditions. Therefore, the rule of the 200-fold factor was enough to determine the UOR_{RIT} from UOR_{Biodis}. However, because tumors were smaller in animals subjected to radioimmunotherapy than in controls, their UOR_{RIT} was calculated by taking also into consideration this weight variation. Hence, the real tumor weight was assessed as follows: UOR_{Biodis} per gram of tumor was calculated by dividing UOR_{Biodis} by the measured tumor weight. This value was then multiplied by the calculated weight of the tumor in radioimmunotherapy conditions (as described in the section Tumor Weight Assessment). This approach was supported by the finding that in biodistribution studies uptake of radioactivity increased linearly with tumor size. Thus, we could extrapolate the UOR from large to small tumors and calculate their UOR_{RIT}. The endpoint of the analysis was calculated by hypothesizing that the remaining activity at 240 h would exponentially decrease to reach a value lower than 1 %IA/g at 700 h.

Dosimetry

The total cumulative decays per tissue were calculated by measuring the area under the UOR_{RIT} curves. Following the MIRD formalism, resulting values were multiplied by the *S* factor. This parameter was calculated by assuming that all the energy delivered at each decay was locally absorbed, and we checked that the contribution of x- and γ-rays could be neglected (*30*). A global energy of 19.483 keV/decay was then considered for calculating the irradiation doses.

Statistical Analysis

A linear mixed-regression model, containing both fixed and random effects (*31,32*), was used to determine the relationship between tumor growth (assessed by bioluminescence imaging) and number of days after grafting. The fixed part of the model included variables corresponding to the number of postgraft days and the different mAbs. Interaction terms were built into the model; random intercepts and random slopes were included to take time into account. The coefficients of the model were estimated by maximum likelihood and considered significant at the 0.05 level.

Survival rates were estimated from the date of the xenograft until the date of the event of interest (i.e., a bioluminescence value of 4.5×10^7 photons/s) using the Kaplan–Meier method. Median survival was presented and survival curves compared using the log-rank test. Statistical analysis was performed using STATA 10.0 software (StataCorp).

RESULTS

Tumor Growth Assessment

The presence of tumor nodules in control mice was observed as early as 3–4 d after the grafting of A-431 cells (Fig. 1A). Total number of tumor nodules per mouse and

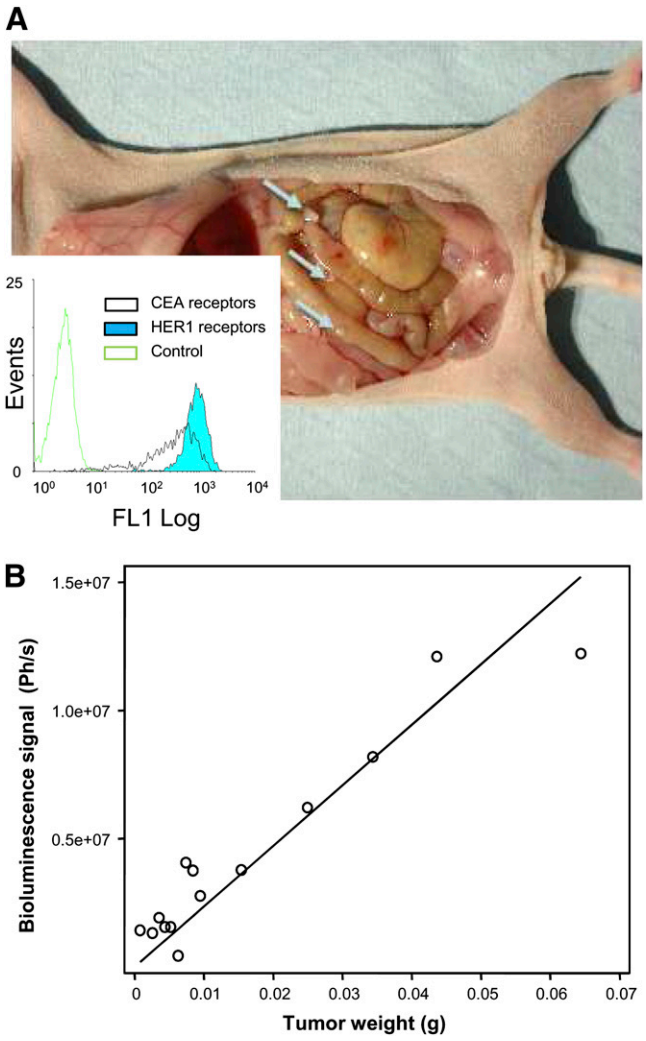

FIGURE 1. Tumor growth and bioluminescence calibration curves. (A) Swiss nude mice bearing 1- to 2-mm xenograft A-431 tumor nodules were followed by bioluminescence imaging. Flow cytometry analysis (inset) indicated similar levels of expression of EGFR and CEA receptors at surface of A-431 cells. (B) In vivo relationship between bioluminescence signal and mean tumor weight per mouse. Ph/s = photons/s.

their size increased with time. For example, the mean number of nodules in control mice was 2.7 ± 0.9 at day 4, 4.8 ± 0.8 at day 7, and 6.6 ± 3 at day 20 after grafting. Mean tumor weight was $1.4 \pm 0.9 \times 10^{-2}$ g at day 4, $4.2 \pm 0.9 \times 10^{-2}$ g at day 7, and $16 \pm 0.7 \times 10^{-2}$ g at day 20. Similar tumor growth rates were observed in mice treated with unlabeled 35A7 or PX mAbs, whereas tumor growth was much slower in the group treated with unlabeled m225. The presence of ascites was never observed throughout the study, and the number of collected nodules always corresponded to the number of bioluminescence spots.

To indirectly measure tumor size in mice subjected to radioimmunotherapy, we calibrated the bioluminescence signal (photons/s) as a function of tumor size. We used a linear relationship to plot the signal intensity of control tumor nodules versus their weight. This procedure was satisfying only for tumors weighing less, or about 1×10^{-1} g (Fig. 1B). For bigger tumor nodules, the dose–response relationship was saturated, and the tumor size was, therefore, underestimated. Indeed, according to the calibration curve, the value of 4.5×10^7 photons/s should correspond to a mean tumor weight of about 2×10^{-1} g, whereas, on dissection, the real tumor weight was $2–3 \times 10^{-1}$ g.

Tumor Growth in Radioimmunotherapy Experiments

Tumor growth followed by bioluminescence imaging (Supplemental Figs. 1A−1C; supplemental materials are available online only at http://jnm.snmjournals.org) rose similarly among mice treated with NaCl or unlabeled PX and 35A7 mAbs (Figs. 2A and 2C). Although no changes in tumor growth were observed with ^{125}I -PX mAbs (Fig. 2C), treatment with ^{125}I-35A7 mAbs slowed tumor growth, and endpoint values of $2–3 \times 10^{-1}$ g were reached only at day 99 after xenografting (Fig. 2A). The internalizing m225 mAbs had a strong inhibitory effect on tumor growth both in the unlabeled and in the labeled forms (Fig. 2B). Indeed, mean tumor weight in mice treated with m225 mAbs remained below 2×10^{-1} g for the entire study, as could be explained by the fact that the growth rate of tumors was slower and more heterogeneous in m225-treated mice than in other groups. Therefore, sacrifice of m225-treated mice was less frequent than that of mice in the other groups, and the highest registered signal did not affect the global mean bioluminescence value of this group.

Survival of Mice Exposed to Therapeutic Activities of ^{125}I-Labeled or Unlabeled mAbs

Mice were sacrificed when the bioluminescence signal reached 4.5×10^7 photons/s. The median survival (MS) was about 19 and 24 d in mice treated with NaCl or unlabeled 35A7, respectively. Conversely, survival was significantly higher in the group treated with ^{125}I-35A7 mAbs (MS, 59 d; $P = 0.0132$) (Fig. 3A). Both unlabeled m225 (MS, 76 d; $P = 0.0014$) and ^{125}I-m225 mAbs (MS, 77 d; $P = 0.9289$) improved survival, compared with NaCl (Fig. 3B).

No statistical difference was observed in the NaCl, 35A7, PX, or ^{125}I-PX groups ($P = 0.3189$ for NaCl vs. 35A7; $P = 0.9046$ for NaCl vs. PX; $P = 0.5109$ for NaCl vs. ^{125}I-PX; $P = 0.5095$ for PX vs. ^{125}I-PX), with an MS of 19, 24, and 17 d, respectively, underscoring the low nonspecific toxicity of ^{125}I-mAb (Fig. 3C).

To cope with the lower toxicity of Auger emitters than β-emitters toward the target tumors and to assess the side effects of repeated injections, a third injection of 37 MBq of ^{125}I-mAbs (m225 or 35A7) was administered at day 10 after xenografting in 2 additional groups of mice. In this case, mice treated with ^{125}I-35A7 mAbs died before the bioluminescence signal reached 4.5×10^7 photons/s, suggesting that the maximum tolerated dose was attained, and MS dropped to 14 d. Conversely, a nonsignificant increase in MS was observed in the ^{125}I-m225 group (MS, ~94 d).

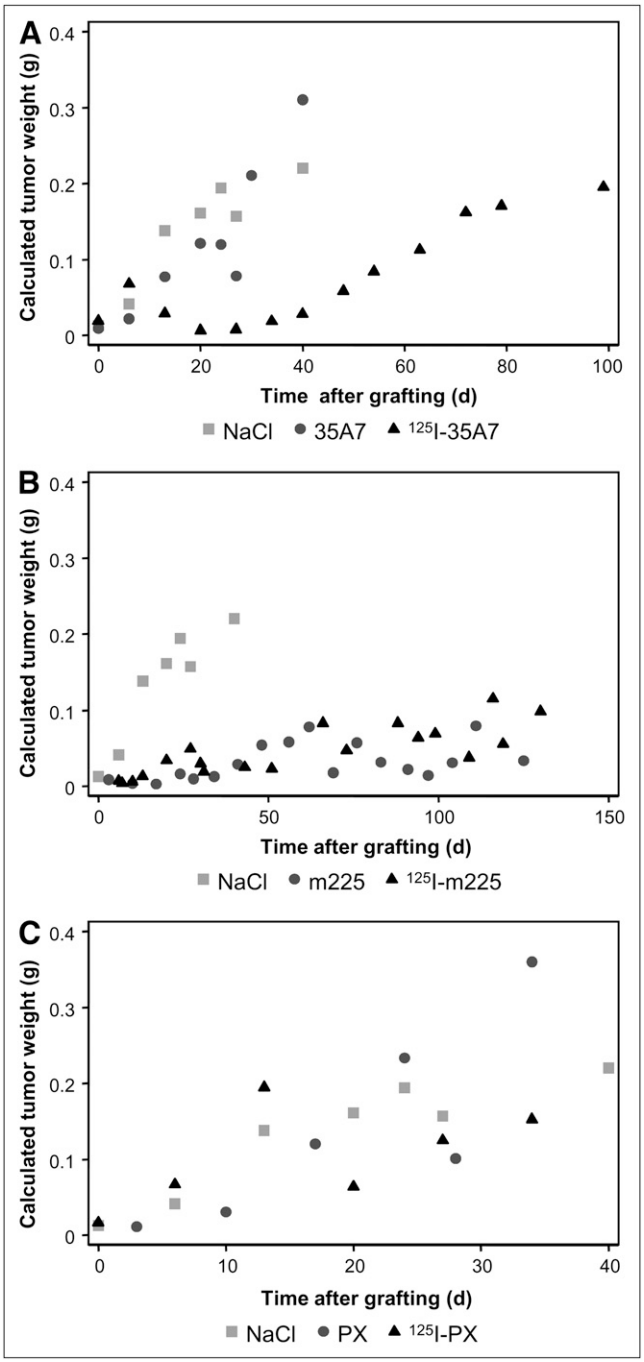

FIGURE 2. Swiss nude mice bearing intraperitoneal A-431 tumor cell xenografts were injected twice with 37 MBq of ^{125}I-mAbs (370 MBq/mg) or with unlabeled mAbs (100 μg). (A) Noninternalizing 35A7 mAbs. (B) Internalizing m225 mAbs. (C) Irrelevant PX mAbs. Untreated controls were injected with NaCl. Tumor growth was followed by bioluminescence imaging. Corresponding mean tumor weights were next calculated using calibration curve reported in Figure 1B, and they are shown as function of time in A, B, C, respectively.

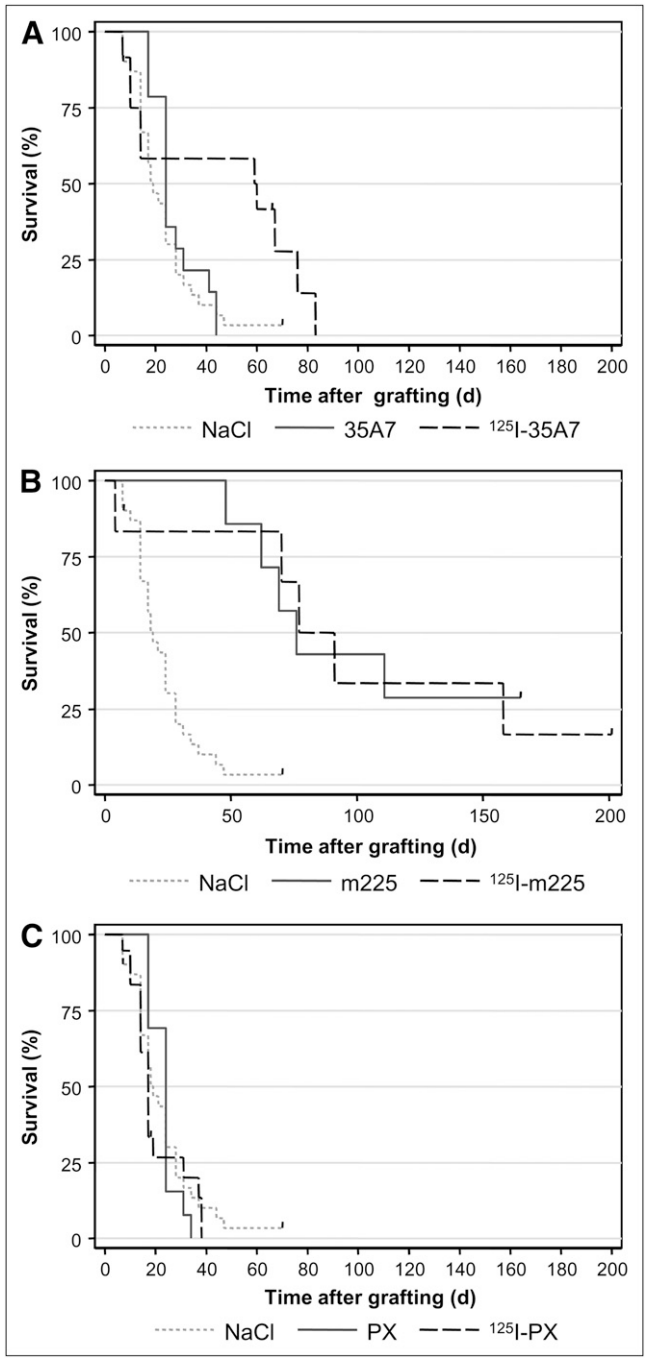

FIGURE 3. Swiss nude mice bearing intraperitoneal A-431 tumor cell xenografts were intravenously injected twice with 37 MBq of ^{125}I-mAbs (370 MBq/mg) or with unlabeled mAb (100 μg). (A) Noninternalizing 35A7 mAbs. (B) Internalizing m225 mAbs. (C) Irrelevant PX mAb. Survival rates were estimated using Kaplan–Meier method. Mice were sacrificed when bioluminescence signal reached 4.5×10^7 photons/s. Censored mice are indicated on graph by vertical bars.

Biodistribution Analysis

After injection of noninternalizing ^{125}I-35A7 mAbs (Fig. 4A), tumor uptake increased progressively from 10.5% at 1 h after injection to 48.1% after 120 h. An intermediary value of 27.8% was observed at 48 h. These results indicate that the maximal uptake of radioactivity per tumor was reached 2 d after the second injection.

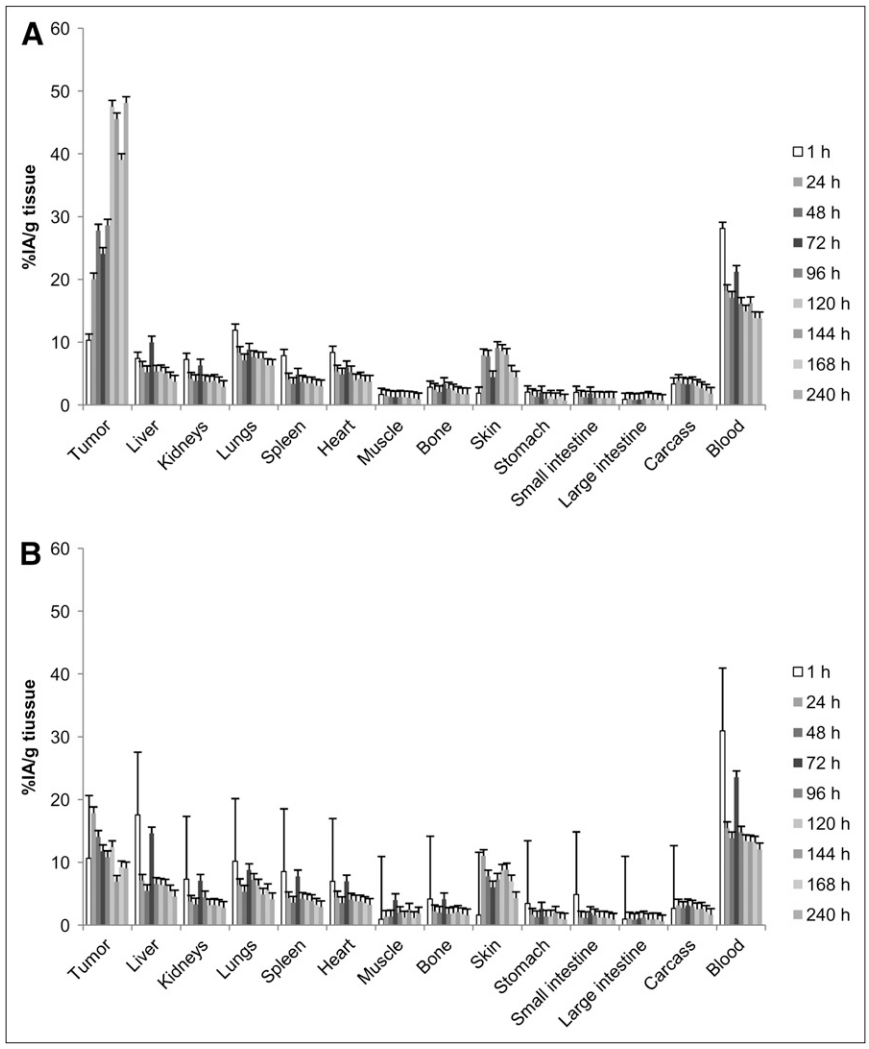

FIGURE 4. Biodistribution. Swiss nude mice bearing intraperitoneal A-431 tumor cell xenografts were intravenously injected twice with solution containing specific ^{125}I-mAbs or irrelevant^{131}I-PX. %IA/g was determined in healthy organs and tumors. (A) Noninternalizing ^{125}I-mAbs. (B) Internalizing ^{125}I-mAbs. Four mice were analyzed at each time point.

Maximal uptake in the blood was 28.1% ± 2.4% and 21.2% ± 1.1% immediately after injections 1 and 2, respectively.

By contrast, tumor uptake of internalizing ^{125}I-m225 mAbs was much lower (Fig. 4B), with a maximal uptake of 17.8% ± 6.8% observed 24 h after injection 1 and no increase after injection 2. Uptake of internalizing ^{125}I-m225 mAbs in the blood, similar to that of noninternalizing mAbs, was maximal immediately after injections 1 and 2, with values of 30.9% ± 3.9% and 23.5% ± 1.2%.

Nonspecific tumor uptake of the ^{131}I-PX mAbs was between 2.8% ± 0.5% and 11.5% ± 4.6% with ^{125}I-35A7 and between 5.9% ± 3.2% and 9.7% ± 1.8% with ^{125}I-m225.

For all the other organs, no significant differences were observed between the 2 targeting models, and values were lower than those measured in tumors and blood.

Uptake of Radioactivity per Organ and Tumor

The uptake of radioactivity per tissue (expressed in becquerels) in radioimmunotherapy experiments (UOR_{RIT}) was extrapolated from the uptake per tissue (UOR_{Biodis}) measured during the biodistribution experiments, and these values were plotted versus time (Figs. 5A and 5B). Both targeting models presented similar UOR_{RIT} values in all tissues analyzed, with the exception of tumors. Carcass, liver, and blood contained the highest peak activity (10–30 MBq) because of their larger volume (Supplemental Figs. 2A and 2B), whereas the other organs showed lower values, generally below 1.7 MBq. Maximal peak uptake by tumors reached values of 1.8 MBq with noninternalizing and 0.05 MBq with internalizing ^{125}I-mAbs. For all the tissues, 2 peak values corresponding to the 2 injections were observed.

Dosimetry

To obtain accurate information about the total energy absorbed by tumors and healthy organs, we calculated their irradiation doses. The highest irradiation doses were delivered to tumors, blood, liver, skin, and lungs, and the lowest were delivered to the small and large intestines and stomach (Fig. 6). Similar irradiation doses were delivered by the 2 targeting models in healthy organs and tissues. Therapy with the internalizing ^{125}I-m225 mAb produced slightly higher irradiation doses in the stomach (+14.4%), liver (+16.3%), kidneys (+3.5%), muscle (+31.8%), small intestine (+1.1%), large intestine (+3.9%), bone (+5.1%),

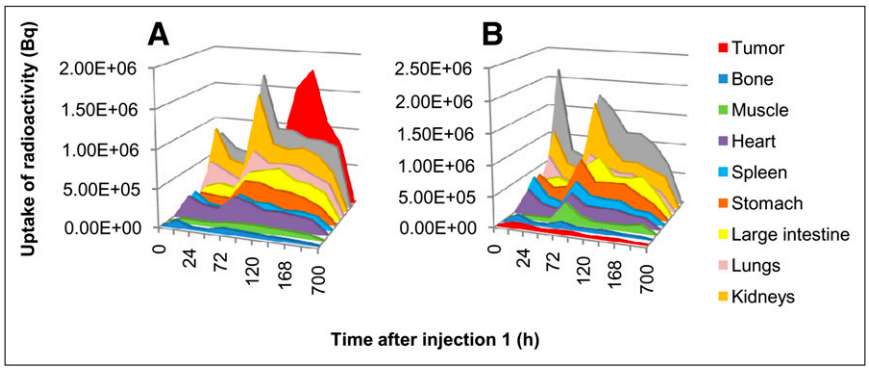

FIGURE 5. Uptake of radioactivity. Uptake of radioactivity per tissue (becquerel) was determined using values obtained during biodistribution experiments (Fig. 4). (A) Noninternalizing ^{125}I-mAbs. (B) Internalizing ^{125}I-mAbs.

and skin (+9.9%). Conversely, lower irradiation doses were calculated for lungs (−7.4%) and blood (−7.0%). For the heart and carcass, less than 1% discrepancy in irradiation doses was determined between both targeting models. However, a huge difference was observed in tumors because internalizing mAbs delivered only 15.1 Gy in comparison to the 111.6 Gy of noninternalizing mAbs.

DISCUSSION

In this study, we investigated the efficiency of ^{125}I-labeled internalizing and noninternalizing mAbs in eradicating small solid intraperitoneal tumors. We showed that labeling of the noninternalizing 35A7 mAb was accompanied by a statistically significant increase in the MS from 24 d (controls) to 59 d. Unlabeled m225 mAb showed by itself a strong efficiency, with an MS of 76 d that was not improved by labeling with ^{125}I.

The standard treatment of patients with peritoneal carcinomatosis is based on cytoreductive surgery, followed by heated intraperitoneal chemotherapy (HIPEC) (*33*); however, several studies have started to compare the efficiency of radioimmunotherapy with HIPEC. For instance, Aarts et al. targeted in rats carcinomatosis of about 1 mm after cytoreductive surgery with radioimmunotherapy or HIPEC. They obtained an MS of 97 d (vs. 57 d in untreated controls) after 1 intraperitoneal injection of 74 MBq of ^{177}Lu- MG1 mAbs and 76 d with HIPEC (*34*). Moreover, Aarts et al. showed that radioimmunotherapy was less detrimental for healthy tissues (*35*). Our study indicates that a significant increase in MS could be achieved also with ^{125}I-mAbs and suggests that ^{125}I-mAbs could be as efficient as ^{177}Lu-mAbs in the case of small tumors.

However, more experiments need to be performed; direct comparison between studies cannot be accurate because of the different experimental models used and, in particular, the possibility of variable radiation sensitivity of the targeted tumor cells.

Compared with conventional, more energetic β-emitters, the interest of Auger electron emitters relies on their low myelotoxicity, which allows repeated injections (*18,19*). Repeated injections are important because it has been speculated that the failure of the phase III trial with ^{90}Y-HMFG1 in ovarian cancers was linked to the low irradiation dose delivered by a single administration (*36*). Therefore, with low-energy Auger electrons the injected activities could be increased to cope with their lower tumor toxicity, and a therapeutic gain of about 2 in comparison to β-emitters has been already demonstrated (*37*). Here, we show that in the mouse 2 injections of 37 MBq of ^{125}I-mAbs are well tolerated and greatly increase MS. However, mice that received a third injection of ^{125}I-35A7 mAbs died before the bioluminescence signal reached 4.5×10^7 photons/s. These results suggest that the maximum tolerated dose was reached and that the maximal therapeutic gain, under our experimental conditions, is obtained with 2 injections of ^{125}I-mAbs over 3 d. Studies are under way to determine the toxic effects on bone marrow of this regimen, although overt signs of myelotoxicity were not observed.

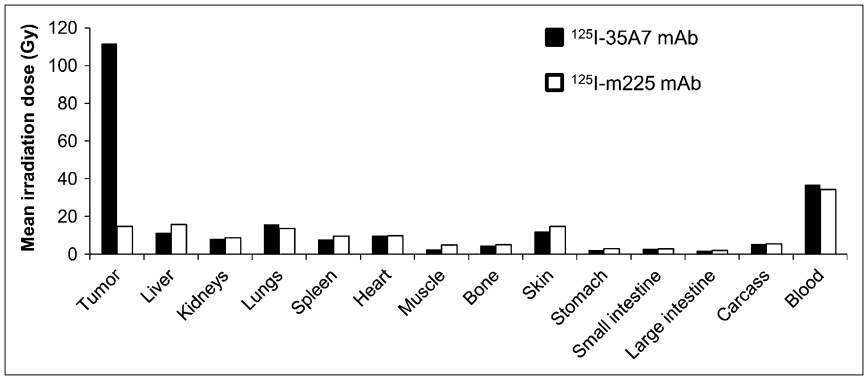

FIGURE 6. MIRD dose calculation. From Figure 5, total cumulative decays per tissue, Ã, was calculated by measuring area under each curve. Ã was next multiplied by 19.483 keV, corresponding to mean energy delivered at each ^{125}I decay.

Conjugation to ^{125}I was accompanied by a significant increase in survival (i.e., 40 d) in the case of the noninternalizing mAb 35A7, whereas labeling did not further increase the positive effect of the internalizing mAb m225. Moreover, the mean irradiation dose for tumors was 111.6 Gy with ^{125}I-35A7 and 15.1 Gy with ^{125}I-m225. These findings indicate that labeling m225 with ^{125}I does not improve its therapeutic efficiency, mainly because the delivered irradiation dose was too low. This was not due to lack of EGFR expression in A-431 cells, because flow cytometry analysis revealed that CEA and *HER1* antigens were expressed at similar levels (Fig. 1A). Because 35A7 and m225 immunoreactivity and immunoaffinity are comparable in vitro, we think that catabolism of internalizing mAbs must have been the cause of the low number of total cumulative decays in tumors treated with ^{125}I-m225, an effect linked to its short retention time within the tumor. Indeed, the %IA/g of tumors reached 48.1% with ^{125}I-35A7 but only 17.8% with ^{125}I-m225. Internalizing ^{125}I-mAbs are catabolized within the cells, and 1 of the catabolism products is a diffusible iodotyrosine moiety. Methodologies aimed at producing residualizing peptides, which can be conjugated to mAbs before the iodination process, have been developed. In this case, catabolism produces iodinated residual peptides that are trapped within the lysosomes to increase tumor retention time (*38–41*). However, with residualizing peptides tumor irradiation could be increased by a factor of 3–4, whereas in our study a 7.4-fold increase (i.e., from 15.1 to 111.6 Gy) was observed with noninternalizing mAbs in comparison to internalizing mAbs. Moreover, the high turnover rate of cell surface antigens represents a limiting factor for mAb penetration within solid tumors (*42*).

Nevertheless, the limits of dosimetry in the case of Auger electrons must be kept in mind. Indeed, because most of the energy is delivered within a sphere of several nanometers around the decay site, the calculation of the mean irradiation dose for an organ or even for a cell could lead to approximations that do not take into account the real dose distribution. If this type of approximation is acceptable in the case of low-LET radiations, such as γ-rays, the correlation between mean irradiation dose and biologic effects must be used carefully in the case of high-LET particles, particularly in the case of low-energy Auger electrons. Indeed, because of the strong heterogeneity of the energy deposits, some areas of a tumor nodule could be not irradiated and cells therein could grow, despite a high mean tumor dose. In our study, mean calculated irradiation doses might appear rather high; this can be explained by the strong initial uptake of ^{125}I-35A7 mAb by tumors (48.1%) that led us to consider a long interval (700 h) before reaching the endpoint of 1 %IA/g of tumor. Then, dose rate is finally rather low and would explain the lack of overt toxicities toward safe tissues. Behr et al. have reported radiation absorbed doses to the blood up to 24.3 Gy in mice administered ^{125}I-CO17-1A mAbs at a maximum tolerated dose of 111 MBq (*18*). These radiation absorbed doses are almost identical to those estimated by us for ^{125}I-35A7 mAb using a similar observation period of 500 h (20.1 Gy) but exceed by about 10-fold those normally found to be dose-limiting for energetic β-emitters, indicating a different relationship between radiation absorbed dose and biologic effect for Auger electron emitters.

Another point could be that inhomogeneous UOR in solid tumors could alter the linearity of the relationship between tumor mass and UOR that was used for dosimetric assessment. Therefore, calculated irradiation doses could be overestimated.

Our study is in agreement with our previous in vitro study showing that the cell membrane (targeted by noninternalizing mAbs) was sensitive to ^{125}I decays (*25*). Noninternalizing ^{125}I-mAbs might produce strong energy deposits, which are localized at the cell membrane, whereas internalizing ^{125}I-mAbs mostly segregate within lysosomes. However, these conclusions probably cannot be extrapolated to other Auger electron emitters, such as ^{111}In, ^{123}I, or ^{67}Ga. Indeed, although their disintegration produces 8, 11, and 20 Auger electrons, respectively, with energy ranging from 12 eV to 24 keV (*43*), their decays are also associated with more or less energetic photon rays or conversion electrons that contribute mostly to the irradiation dose. For this reason, ^{125}I can be considered the Auger electron emitter that produces the most localized energy deposits and the lowest toxic side effects. One of the main drawbacks of ^{125}I for clinical use is its rather long physical period. However, this could be minimized if ^{125}I-mAbs were administered after HIPEC, because the latter procedure allows the removal of non–cell-bound radiolabeled antibody from the peritoneal cavity.

CONCLUSION

We have shown that growth of solid tumors can be significantly reduced and survival of mice improved by radioimmunotherapy with ^{125}I-labeled noninternalizing mAbs.

Catabolism of internalizing ^{125}I-mAbs, labeled with nonresidualizing methods, release diffusible iodotyrosine moieties. This release might explain the drastically reduced efficiency of these antibodies in our study, preventing accurate comparison between cytoplasmic and cell surface localizations. However, these results confirm our previous in vitro work showing that the cell membrane is sensitive to ^{125}I decays. The results indicate that the use of internalizing mAbs, which drive radioactivity in cells near the nucleus, is not a prerequisite to the success of therapy with ^{125}I.

ACKNOWLEDGMENTS

We thank Imade Ait Arsa for animal care and involvement in experiments. This work was supported by the Electricité de France-Service de Radioprotection.

REFERENCES

1. Davies AJ. Radioimmunotherapy for B-cell lymphoma: Y90 ibritumomab tiuxetan and I^{131} tositumomab. *Oncogene.* 2007;26:3614–3628.

2. Oei AL, Verheijen RH, Seiden MV, et al. Decreased intraperitoneal disease recurrence in epithelial ovarian cancer patients receiving intraperitoneal consolidation treatment with yttrium-90-labeled murine HMFG1 without improvement in overall survival. *Int J Cancer.* 2007;120:2710–2714.
3. Verheijen RH, Massuger LF, Benigno BB, et al. Phase III trial of intraperitoneal therapy with yttrium-90-labeled HMFG1 murine monoclonal antibody in patients with epithelial ovarian cancer after a surgically defined complete remission. *J Clin Oncol.* 2006;24:571–578.
4. Koppe MJ, Postema EJ, Aarts F, Oyen WJ, Bleichrodt RP, Boerman OC. Antibody-guided radiation therapy of cancer. *Cancer Metastasis Rev.* 2005;24: 539–567.
5. Jain RK. Lessons from multidisciplinary translational trials on anti-angiogenic therapy of cancer. *Nat Rev Cancer.* 2008;8:309–316.
6. Williams LE, Bares RB, Fass J, Hauptmann S, Schumpelick V, Buell U. Uptake of radiolabeled anti-CEA antibodies in human colorectal primary tumors as a function of tumor mass. *Eur J Nucl Med.* 1993;20:345–347.
7. Jain M, Venkatraman G, Batra SK. Optimization of radioimmunotherapy of solid tumors: biological impediments and their modulation. *Clin Cancer Res.* 2007;13:1374–1382.
8. Jain R. Physiological barriers to delivery of monoclonal antibodies and other macromolecules in tumors. *Cancer Res.* 1990;50(3 suppl):814s−819s.
9. Thurber GM, Zajic SC, Wittrup KD. Theoretic criteria for antibody penetration into solid tumors and micrometastases. *J Nucl Med.* 2007;48:995–999.
10. Sharkey RM, Pykett MJ, Siegel JA, Alger EA, Primus FJ, Goldenberg DM. Radioimmunotherapy of the GW-39 human colonic tumor xenograft with ^{131}I-labeled murine monoclonal antibody to carcinoembryonic antigen. *Cancer Res.* 1987;47:5672–5677.
11. Koppe M. Radioimmunotherapy and colorectal cancer. *Br J Surg.* 2005;92: 264–276.
12. Behr TM, Liersch T, Greiner-Bechert L, et al. Radioimmunotherapy of small-volume disease of metastatic colorectal cancer. *Cancer.* 2002;94(4, suppl):1373–1381.
13. Sharkey RM, Weadock KS, Natale A, et al. Successful radioimmunotherapy for lung metastasis of human colonic cancer in nude mice. *J Natl Cancer Inst.* 1991;83:627–632.
14. Vogel CA, Galmiche MC, Buchegger F. Radioimmunotherapy and fractionated radiotherapy of human colon cancer liver metastases in nude mice. *Cancer Res.* 1997;57:447–453.
15. Couturier O, Supiot S, Degraef-Mougin M, et al. Cancer radioimmunotherapy with α-emitting nuclides. *Eur J Nucl Med Mol Imaging.* 2005;32:601–614.
16. Sofou S, Kappel BJ, Jaggi JS, McDevitt MR, Scheinberg DA, Sgouros G. Enhanced retention of the α-particle-emitting daughters of actinium-225 by liposome carriers. *Bioconjug Chem.* 2007;18:2061–2067.
17. Kassis AI. Radiotargeting agents for cancer therapy. *Expert Opin Drug Deliv.* 2005;2:981–991.
18. Behr TM, Sgouros G, Vougiokas V, et al. Therapeutic efficacy and dose-limiting toxicity of Auger-electron vs. β emitters in radioimmunotherapy with internalizing antibodies: evaluation of ^{125}I- vs. ^{131}I-labeled CO17-1A in a human colorectal cancer model. *Int J Cancer.* 1998;76:738–748.
19. Behr TM, Behe M, Lohr M, et al. Therapeutic advantages of Auger electron-over β-emitting radiometals or radioiodine when conjugated to internalizing antibodies. *Eur J Nucl Med.* 2000;27:753–765.
20. Michel RB, Brechbiel MW, Mattes MJ. A comparison of 4 radionuclides conjugated to antibodies for single-cell kill. *J Nucl Med.* 2003;44:632–640.
21. Michel RB, Castillo ME, Andrews PM, Mattes MJ. In vitro toxicity of A-431 carcinoma cells with antibodies to epidermal growth factor receptor and epithelial glycoprotein-1 conjugated to radionuclides emitting low-energy electrons. *Clin Cancer Res.* 2004;10:5957–5966.
22. Kassis AI, Adelstein SJ. Radiobiologic principles in radionuclide therapy. *J Nucl Med.* 2005;46(suppl 1):4S–12S.
23. Hofer KG. Biophysical aspects of Auger processes. *Acta Oncol.* 2000;39: 651–657.
24. Hofer KG, Lin X, Schneiderman MH. Paradoxical effects of iodine-125 decays in parent and daughter DNA: a new target model for radiation damage. *Radiat Res.* 2000;153:428–435.
25. Pouget JP, Santoro L, Raymond L, et al. Cell membrane is a more sensitive target than cytoplasm to dense ionization produced by auger electrons. *Radiat Res.* 2008;170:192–200.
26. Pelegrin A, Terskikh A, Hayoz D, et al. Human carcinoembryonic antigen cDNA expressed in rat carcinoma cells can function as target antigen for tumor localization of antibodies in nude rats and as rejection antigen in syngeneic rats. *Int J Cancer.* 1992;52:110–119.
27. Pillon A, Servant N, Vignon F, Balaguer P, Nicolas JC. In vivo bioluminescence imaging to evaluate estrogenic activities of endocrine disrupters. *Anal Biochem.* 2005;340:295–302.
28. Hammarstrom S, Shively JE, Paxton RJ, et al. Antigenic sites in carcinoembryonic antigen. *Cancer Res.* 1989;49:4852–4858.
29. Kohler G, Howe SC, Milstein C. Fusion between immunoglobulin-secreting and nonsecreting myeloma cell lines. *Eur J Immunol.* 1976;6:292–295.
30. Boutaleb S, Pouget JP, Hindorf C, et al. Impact of mouse model on pre-clinical dosimetry in Targeted Radionuclide Therapy. *Proc IEEE.* In press.
31. McCulloch CE, Searle SR. *Generalized, Linear, and Mixed Models.* New York, NY: Wiley-Interscience; 2001.
32. Laird NM, Ware JH. Random-effects models for longitudinal data. *Biometrics.* 1982;38:963–974.
33. Ceelen WP, Hesse U, de Hemptinne B, Pattyn P. Hyperthermic intraperitoneal chemoperfusion in the treatment of locally advanced intra-abdominal cancer. *Br J Surg.* 2000;87:1006–1015.
34. Aarts F, Hendriks T, Boerman OC, Koppe MJ, Oyen WJ, Bleichrodt RP. A comparison between radioimmunotherapy and hyperthermic intraperitoneal chemotherapy for the treatment of peritoneal carcinomatosis of colonic origin in rats. *Ann Surg Oncol.* 2007;14:3274–3282.
35. Aarts F, Bleichrodt RP, de Man B, Lomme R, Boerman OC, Hendriks T. The effects of adjuvant experimental radioimmunotherapy and hyperthermic intraperitoneal chemotherapy on intestinal and abdominal healing after cytoreductive surgery for peritoneal carcinomatosis in the rat. *Ann Surg Oncol.* 2008;15:3299–3307.
36. Meredith RF, Buchsbaum DJ, Alvarez RD, LoBuglio AF. Brief overview of preclinical and clinical studies in the development of intraperitoneal radioimmunotherapy for ovarian cancer. *Clin Cancer Res.* 2007;13:5643s–5645s.
37. Barendswaard EC, Humm JL, O'Donoghue JA, et al. Relative therapeutic efficacy of ^{125}I- and ^{131}I-labeled monoclonal antibody A33 in a human colon cancer xenograft. *J Nucl Med.* 2001;42:1251–1256.
38. Stein R, Govindan SV, Mattes MJ, et al. Improved iodine radiolabels for monoclonal antibody therapy. *Cancer Res.* 2003;63:111–118.
39. Vaidyanathan G, Affleck DJ, Bigner DD, Zalutsky MR. Improved xenograft targeting of tumor-specific anti-epidermal growth factor receptor variant III antibody labeled using *N*-succinimidyl 4-guanidinomethyl-3-iodobenzoate. *Nucl Med Biol.* 2002;29:1–11.
40. Sharkey RM, Karacay H, Cardillo TM, et al. Improving the delivery of radionuclides for imaging and therapy of cancer using pretargeting methods. *Clin Cancer Res.* 2005;11:7109s–7121s.
41. Kurth M, Pelegrin A, Rose K, et al. Site-specific conjugation of a radioiodinated phenethylamine derivative to a monoclonal antibody results in increased radioactivity localization in tumor. *J Med Chem.* 1993;36:1255–1261.
42. Ackerman ME, Pawlowski D, Wittrup KD. Effect of antigen turnover rate and expression level on antibody penetration into tumor spheroids. *Mol Cancer Ther.* 2008;7:2233–2240.
43. Kassis AI. Cancer therapy with Auger electrons: are we almost there? *J Nucl Med.* 2003;44:1479–1481.